Journal of Energy Chemistry 91 (2024) 512–521

Contents lists available at ScienceDirect

Journal of Energy Chemistry

journal homepage: www.elsevier.com/locate/jechem

http://www.journals.elsevier.com/journal-of-energy-chemistry/

Accurate and efficient remaining useful life prediction of batteries enabled by physics-informed machine learning

Liang Ma [a], Jinpeng Tian [b,*], Tieling Zhang [a,*], Qinghua Guo [c], Chunsheng Hu [d]

[a] School of Mechanical, Materials, Mechatronic and Biomedical Engineering, University of Wollongong, Wollongong, NSW 2522, Australia
[b] Department of Electrical and Electronic Engineering and Research Centre for Grid Modernization, The Hong Kong Polytechnic University, Kowloon, Hong Kong 999077, China
[c] School of Electrical, Computer and Telecommunications Engineering, University of Wollongong, Wollongong, NSW 2522, Australia
[d] School of Advanced Interdisciplinary Studies, Ningxia University, Yinchuan 750000, Ningxia, China

ARTICLE INFO

Article history:
Received 2 December 2023
Revised 29 December 2023
Accepted 30 December 2023
Available online 11 January 2024

Keywords:
Lithium-ion batteries
Remaining useful life
Physics-informed machine learning

ABSTRACT

The safe and reliable operation of lithium-ion batteries necessitates the accurate prediction of remaining useful life (RUL). However, this task is challenging due to the diverse ageing mechanisms, various operating conditions, and limited measured signals. Although data-driven methods are perceived as a promising solution, they ignore intrinsic battery physics, leading to compromised accuracy, low efficiency, and low interpretability. In response, this study integrates domain knowledge into deep learning to enhance the RUL prediction performance. We demonstrate accurate RUL prediction using only a single charging curve. First, a generalisable physics-based model is developed to extract ageing-correlated parameters that can describe and explain battery degradation from battery charging data. The parameters inform a deep neural network (DNN) to predict RUL with high accuracy and efficiency. The trained model is validated under 3 types of batteries working under 7 conditions, considering fully charged and partially charged cases. Using data from one cycle only, the proposed method achieves a root mean squared error (RMSE) of 11.42 cycles and a mean absolute relative error (MARE) of 3.19% on average, which are over 45% and 44% lower compared to the two state-of-the-art data-driven methods, respectively. Besides its accuracy, the proposed method also outperforms existing methods in terms of efficiency, input burden, and robustness. The inherent relationship between the model parameters and the battery degradation mechanism is further revealed, substantiating the intrinsic superiority of the proposed method.

1. Introduction

1.1. Background and literature review

Lithium-ion batteries are playing an increasingly important role in achieving the goal of carbon neutrality, with their applications ranging from electric vehicles to grid energy storage. They have the advantages of high energy density, long lifespan, and low self-discharge rate [1,2]. However, lithium-ion batteries suffer from various degradation modes, such as loss of active material (LAM) and loss of lithium inventory (LLI) [3]. Accurate prediction of battery health degradation is therefore of great significance to improve not only battery management but also battery design [4]. The prediction results can ensure timely adjustment of management strategies to avoid accelerated degradation [5] and accelerate the design of new battery chemistries [6].

A battery is recognised as reaching its end of life (EoL) when its capacity is reduced by 20%, for example. The remaining useful life (RUL) is, therefore, an important metric to indicate the health status of the battery. However, predicting the RUL is challenging due to complex battery ageing mechanisms and dynamic usage patterns [7–9]. This issue is compounded by the fact that only current and voltage are regularly measured in realistic battery management systems.

Model-based and data-driven methods have recently attracted research interest in battery RUL prediction. Typical model-based methods include the semi-empirical model [10], the electrochemical model [11], and the equivalent circuit model [12]. The semi-empirical model empirically characterises the relationship between capacity loss and cycle number, considering the ageing

* Corresponding authors.
E-mail addresses: jinpeng.tian@polyu.edu.hk (J. Tian), tieling@uow.edu.au (T. Zhang).

https://doi.org/10.1016/j.jechem.2023.12.043

mechanisms and operational conditions. Han et al. [13] modelled the capacity loss as an exponential function of cycle number, incorporating activation energy, temperature, and gas constant as model parameters to accommodate operating conditions. The electrochemical model and equivalent circuit model are generally implemented by combining battery models with filters [10]. The parameters associated with battery degradation are identified and extrapolated to predict the RUL. For example, Lyu et al. [14] predicted RUL by combining the electrochemical model and a particle filter method. They identified five degradation-related parameters from the electrochemical model over the first 50 cycles. The parameters serve as state variables of the particle filter to predict the cycle number before capacity exceeds a threshold, corresponding to the RUL. Guha et al. [15] developed a fractional order equivalent circuit model, whose parameters were used to reconstruct the internal resistance. They derived a regression function to describe the growth of the internal resistance. After that, a particle filter was employed to update the function parameters to predict the RUL at the present cycle. Although the model-based methods can provide an intuitive understanding of the electrochemical and physical processes of battery operation, the model parameters are obtained based on specific tests, making it difficult to track the battery degradation in varying environments [16,17].

Motivated by the rapid development of artificial intelligence in various fields, such as chemistry [18], materials [19], and bioengineering [20], data-driven methods have attracted increasing attention in RUL prediction [21–24]. Their implementation begins with feature acquisition, based on which a machine learning model is trained for RUL prediction. For example, Severson et al. [25] used the statistical features of change in the voltage-capacity curves to train an elastic net to predict the battery life. They achieved impressive battery life prediction accuracy using data collected from only 100 cycles. On this basis, many studies advanced the prediction performance by proposing more powerful features that can be obtained with fewer data. Howey et al. [26] developed a Bayesian hierarchical linear model to cluster the cycling conditions from 100 cycles before a regression. The results suggest that informative features can improve RUL prediction even when the number is decreased. Liu et al. [17] exploited the seasonal and trend decomposition using the loess technique to extract features from battery cycling curves to predict the RUL. Their results reveal that RUL can be accurately predicted using degradation data before 10% capacity loss for training. In addition to focusing on developing advanced neural networks, extracting more interpretable features attracts increasing attention in data-driven RUL prediction. Wang et al. [27] picked out 7 statistical features from a library of 206 features to describe battery ageing. Though the selected statistical features are generally utilised to depict signal variations, they cannot provide deep insights into battery degradation owing to their ignorance of the degradation mechanisms. Roman et al. [28] extracted 30 features from constant current and constant voltage segments to estimate battery degradation. Jiang et al. [29] utilised cycling data of 30 cycles to predict future capacity degradation, and the features include capacity, charging duration, resistance, and incremental capacity (IC) features. Similarly, these features are statistical values and mathematical transformations of current, voltage, capacity, and energy. Their work builds the relationship between battery operational data and degradation to a certain extent, but the absence of domain knowledge hinders the pace of further improvement.

By leveraging deep learning (DL), quick prediction of RUL using even less data has been achieved. For instance, Wang et al. [30] established a convolutional neural network (CNN) that highlights automatic feature extraction and regression to predict the RUL. The results show that the RUL can be accurately predicted using raw charging and discharging data collected in five consecutive cycles as the input. Based on CNN, Hsu et al. [31] also enabled the prediction of RUL using data from one cycle only and the prediction accuracy was higher than the original research based on 100 cycles by Severson et al. [25]. Tian et al. [32] proposed to predict the voltage-capacity curves in the future 300 cycles by establishing a sequence-to-sequence deep neural network (DNN) that takes the only one curve in the present cycle as the input.

1.2. Gap analysis and our contributions

These studies suggest that battery voltage-capacity curves are highly informative in predicting the RUL, and even data from one cycle can enable accurate prediction of battery RUL. However, it is still doubtful if the combination of raw data and deep learning is the best choice. Data-driven methods are "black-boxes" that map the input to the output without knowing their specific mechanisms. However, the training data of the data-driven methods greatly affect their performance, which inspires us to consider making some contributions to the input data rather than developing a complex neural network. We aim to extract more representative information from the raw data to guide the work of the deep neural network for a specific task, i.e. the RUL prediction in this work.

Inspired by the superiority of physical-guided data-driven methods in other research areas [33,34], we propose a physics-informed method to fuse battery physics and machine learning to accurately predict the battery RUL using data from one cycle only. Ageing-correlated parameters are obtained from mathematically modelling the constant current (CC) charging process of the battery, based on which an accurate prediction of battery lifetime is enabled by the subsequent deep learning. Our contributions are outlined as follows.

(1) A physics-informed machine learning method is proposed to enable accurate and efficient prediction of battery RUL. By using a physics-based model to extract ageing-correlated parameters from battery charging data, the prediction accuracy and efficiency are significantly improved.
(2) The proposed method can adapt to various operating conditions, including different temperatures and charging rates. In addition, the method can maintain high accuracy even in a partial charging situation, offering high flexibility to batteries in service.

The proposed method is systematically validated by considering battery materials, temperature, and current rate factors. The results show that the proposed method outperforms the state-of-the-art fully data-driven approaches in terms of accuracy, efficiency, input burden, and robustness.

1.3. Article organisation

The remainder of this paper is organised as follows. Section 2 introduces the battery degradation data. Section 3 provides an overview of the proposed methodology. Section 4 discusses the validation results. Conclusions are summarised in Section 5.

2. Data generation

Three datasets developed by Zhu et al. [35] are used to evaluate the proposed RUL prediction method, and the cathode materials include $LiNi_{0.86}Co_{0.11}Al_{0.03}O_2$ (NCA), $LiNi_{0.83}Co_{0.11}Mn_{0.07}O_2$ (NCM), and 42(3) wt% $Li(NiCoMn)O_2$ blended with 58(3) wt% $Li(NiCoAl)O_2$ (NCA&NCM). These three kinds of batteries are tested under different temperatures and current rates from their beginning of life

(BoL) to EoL. The specifications of the three types of batteries are summarised in Table S1. The dataset covers plenty of operating conditions to reflect the variability of battery degradation as a function of chemistry, temperature, and current rates. We name the operating condition XX_YY_ZZ, where XX means the cathode material, YY is the temperature, and ZZ represents the charging current rate. For example, NCA_25_0.5 represents an NCA battery tested at 25 °C with a charging rate of 0.5 C. We visualise the voltage and current data from one cycle of NCA_25_0.5 in Fig. 1(a). Each cycle comprises five stages, including constant current charging, constant voltage charging, charging relaxation, constant current discharging, and discharging relaxation. The battery is charged with constant current until the voltage reaches the upper limit and then holds the voltage until the current is reduced to 0.05 C. This process is denoted by stages I and II. In stage IV, the battery is discharged with constant current until the voltage reaches the lower limit. The battery rests for a period after the charging and discharging processes, which are indicated by stages III and V, respectively. Since constant current charging is the most prevalent in daily battery usage [36–38], we follow the previous works [39] and use the constant current charging stage of a cycle to predict the RUL.

The capacity vs. voltage (Q-V) curves of the NCA battery over its life are depicted in Fig. 1(b). It shows that the capacity gradually decreases at the same voltage point from the BoL to the EoL, indicating a significant correlation between the Q-V curves and battery degradation.

The original datasets are displayed in Fig. S1. The datasets are cleaned to collect valid data because some batteries have not declined to 80% of their initial capacity. Some test situations are excluded since the insufficient data volume, such as the NCM battery tested under 35 °C contains only two battery tests. After being screened out, the data used for validating our case is summarised in Table 1 and their capacity trajectories are illustrated in Fig. 1(c–e). There are a total of 72 cells available for method validation, covering three kinds of cathode materials, three temperatures, and two charging current rates. Besides, the battery life and ageing trajectory even vary under the same operational condition, making it tough to predict the RUL.

3. Methodology

This section first introduces the overall framework of the prevalent DL-based RUL prediction methods based on charging curves, from which the research gap is identified. Afterwards, details of the proposed method are elaborated.

3.1. The overall RUL prediction scheme

The DL method generally maps the capacity sequences to the present RUL through a DNN. The mapping relationship can be mathematically described as follows

$$z_i = f_{\mathrm{DNN}}(Q_i(V)) \tag{1}$$

where z denotes the RUL and $Q_i(V)$ is the capacity sequence calculated by the Ampere-hour counting method [40,41], corresponding to an invariant voltage sequence over the Q-V curves. V refers to voltage and i is the cycle number. $f_{\mathrm{DNN}}(\cdot)$ is the mapping established by training a DNN. This framework is widely applied for battery health prognosis, as demonstrated in recent studies [42–44]. Nonetheless, DNN is a 'black box', learning from only the provided training data. Thus, its performance can be compromised if uninformative data are provided as the input. In the context of battery RUL prediction, the conventional framework in Eq. (1) ignores the underlying patterns in the variations of charging curves, which have already been understood and modelled from an electrochemical point of view. To address this issue, we propose to embed the domain knowledge into the input to improve the RUL prediction performance, resulting in the framework described as

$$\begin{cases} \delta_i = P(V_i, Q_i) \\ z_i = f_{\mathrm{DNN}}(\delta_i) \end{cases} \tag{2}$$

where $P(\cdot)$ is a physics-based model that characterises the ageing behaviour of charging curves and the information is encoded into a parameter set δ_i. V refers to the voltage. The difference between the proposed method and conventional methods is the δ_i in Eq. (2). As mentioned above, previous work defines the δ_i in statistical or mathematical transformation ways. Instead of learning from the

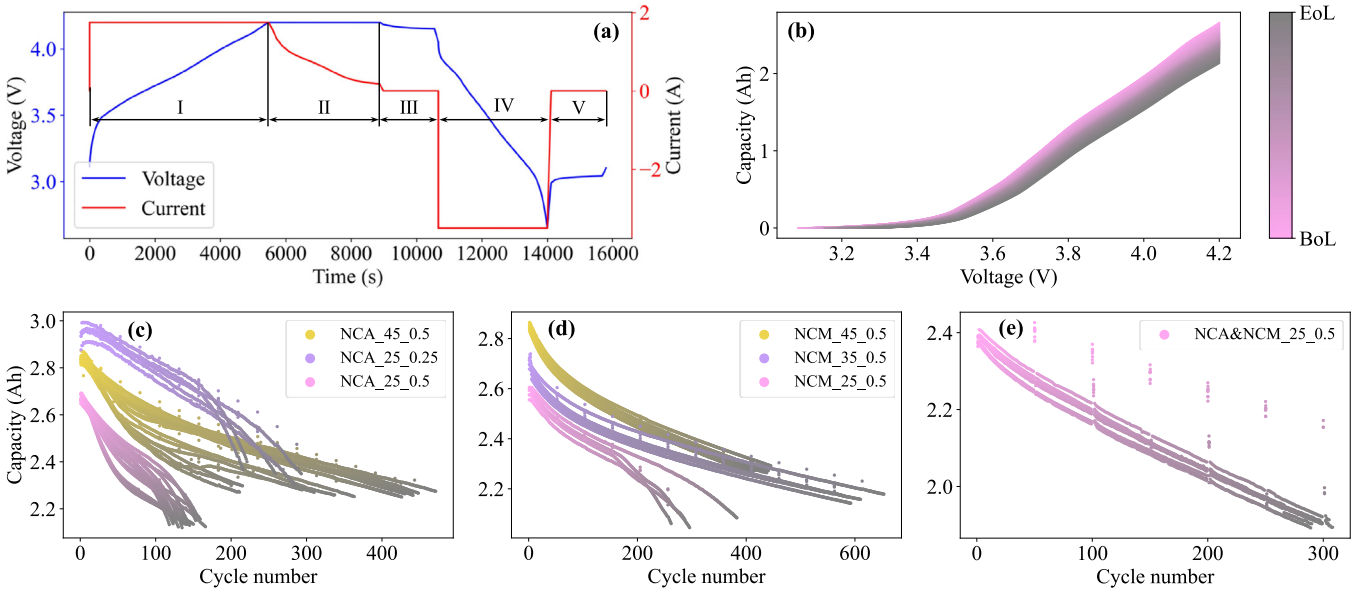

Fig. 1. The obtained battery degradation datasets for method validation. (a) The current and voltage profile of a complete cycle of NCA_25_0.5; (b) the Q-V curves of the constant current charging process over the NCA_25_0.5 battery life; (c–e) degradation trajectories of the NCA, the NCM, and the NCA&NCM batteries.

Table 1
Battery degradation datasets used for model development and validation.

Dataset	Cell chemistry	Temperature (°C)	Charging rate (C)	Number of cells	Operating condition
1	NCA	25	0.5	15	NCA_25_0.5
		25	0.25	5	NCA_25_0.25
		45	0.5	23	NCA_45_0.5
2	NCM	25	0.5	4	NCM_25_0.5
		35	0.5	4	NCM_35_0.5
		45	0.5	12	NCM_45_0.5
3	NCA&NCM	25	0.5	9	NCA&NCM_25_0.5

scratch, the DNN in the proposed framework leverages the physics-based model, so that domain knowledge can be incorporated, leading to significant performance improvement.

The overview of our method is illustrated in Fig. 2. First, we develop an interpretable voltage-capacity model to analyse battery degradation. In this way, the raw operation data are transformed into parameters that govern battery ageing evolution. Second, the model parameters are identified for guiding the following DNN. Third, a DNN is developed and trained using the identified parameters. Thereby, the trained model masters the possible battery ageing evolution. Finally, the trained DNN is deployed for online RUL prediction considering various situations. Details of each part are discussed in the following subsections.

3.2. Physics-based model development

3.2.1. Physical basis of the model

The battery charging and discharging processes can be described as the Li^+ reversibly inserting/extracting into/from the anode and cathode at the level of material. Thus, there exists a close relationship between electrode potential and Li^+ content of active material. This gives rise to the voltage plateaus on the charging curves, which can be amplified through the IC analysis [45]. It has been extensively demonstrated that the peaks of IC curves are highly sensitive to battery degradation [46,47]. For example, the symmetry centre, width, height, and area information derived from IC peaks are associated with the realistic phase transition behaviours of the active material. Thus, it is promising to model the charging curves from the viewpoint of IC transform.

According to the shape of the IC peaks, IC curves can be approximated by the sum of Lorentzian functions [48], which is expressed as follows

$$\frac{dQ}{dV} = \sum_{i=1}^{n} \frac{2A_i}{\pi} \frac{\omega_i}{\omega_i^2 + (2V - 2V_{oi})^2} \tag{3}$$

where n is the number of peaks, A_i is the area of the peak i, ω_i is the width at half-height of the peak i, and V_{oi} is the symmetric centre of the peak i. V represents the collected voltage, while Q is the capacity.

It is noted that errors can be introduced by dQ/dV process mentioned above. To avoid this, integration is performed as Eq. (3)

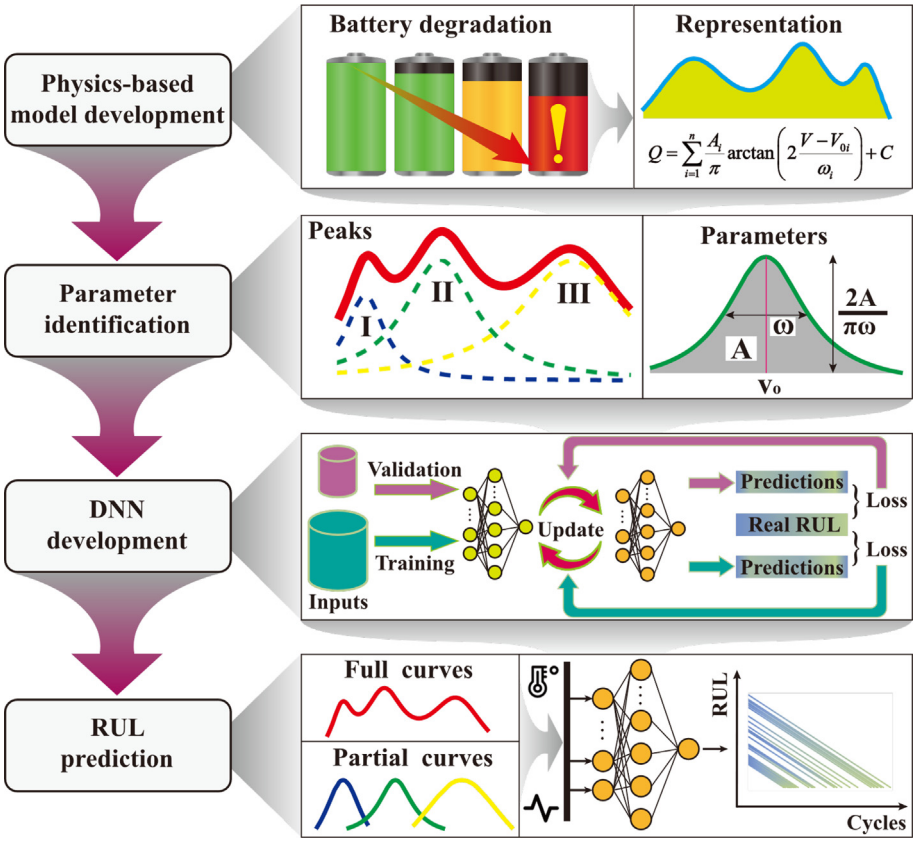

Fig. 2. The overall framework of the proposed methodology.

$$Q = \sum_{i=1}^{n} \frac{A_i}{\pi} \arctan\left(2\frac{V - V_{oi}}{\omega_i}\right) + \mathrm{C} \tag{4}$$

where C is a constant. The model has a total of $(3n + 1)$ parameters and it is beneficial to RUL prediction in two ways.

(1) The model extracts ageing-correlated parameters, improving the interpretability of the input of DL methods for RUL prediction.
(2) As the operational raw data are represented by lower-dimensional parameters, the estimation efficiency of the DL-based RUL prediction can be improved.

3.2.2. Parameter identification and evaluation

The peak number n is determined before parameter identification. Fig. S2 displays the IC curves of the raw datasets under different conditions. Three distinct peaks appear in the curves over the battery life, thus $n = 3$ in Eq. (4) is used to identify the parameters. We label the three peaks as peak 1, peak 2, and peak 3, respectively. Based on the operational capacity and voltage data, the model is parameterized by the nonlinear least squares (NLS) method.

The voltage and current are sampled by sensors during the charging process. The capacity Q is computed as follows

$$Q(V) = \int_{V(t)=V_{\mathrm{low}}}^{V(t)=V} I(t)\mathrm{d}t \tag{5}$$

where V and I are voltage and current, V_{low} is the lower voltage limit. We sample the voltage with a given step ΔV, resulting in a voltage sequence $V = [V_{\mathrm{low}}, V_{\mathrm{low}} + \Delta V, \cdots, V_{\mathrm{low}} + s\Delta V]$, where s is the number of samples calculated by $s = (V_{\mathrm{up}} - V_{\mathrm{low}})/\Delta V$, and V_{up} is the upper voltage limit. The voltage-capacity curve at each cycle then can be expressed as $\{(V_0, Q_0), (V_1, Q_1), (V_2, Q_2), \cdots, (V_s, Q_s)\}$. The parameter identification is to obtain the model parameters by minimising the squared errors, i.e.

$$\delta_i = \mathrm{argmin} \sum_{i=0}^{s} \left(Q_i - f(V_i, \delta_i)\right)^2, \quad s.t.\ \delta_i \epsilon \left(\delta_{\mathrm{up}}, \delta_{\mathrm{low}}\right) \tag{6}$$

where δ is the model parameters, $f(\cdot)$ is the model function, and δ_{up} and δ_{low} are the upper and lower bounds of the parameters, respectively. The boundaries of the model parameters are summarised in Table S2.

The reconstructed Q-V curves using the identified model parameters at the first and last cycle and simulation errors of NCA_25_0.5, NCM_25_0.5, and NCA&NCM_25_0.5 batteries are displayed in the first two rows of Fig. 3. The distinct cathode materials of the three batteries result in different simulation accuracy. Nonetheless, the overall errors of the first and last cycle are within 0.05 Ah (about 2% of the nominal capacity), demonstrating an accurate identification. Moreover, as the adopted V-Q model is based on IC transform, the IC curves can be analytically obtained, as plotted in the third row of Fig. 3, which suggests a more regular variation of peak parameters than the raw-data-based IC curves over the battery life. The root mean squared error (RMSE) and R-squared (R^2) are used to assess the overall errors and goodness of fit, which are calculated by the following equation

$$\begin{cases} RMSE = \sqrt{\frac{1}{k}\sum_{i=1}^{k}\left(Q_i - \widehat{Q}_i\right)^2} \\ R^2 = 1 - \frac{\sum_{i=1}^{k}\left(Q_i - \widehat{Q}_i\right)^2}{\sum_{i=1}^{k}\left(Q_i - \bar{Q}\right)^2} \end{cases} \tag{7}$$

where Q and $\widehat{Q}$ are the real capacity and simulated capacity, respectively. $\bar{Q}$ is the mean value of the real capacity, and k is the number of samples of a cycle. The RMSE and R^2 are shown in Fig. S3, which demonstrates high identification accuracy.

3.3. Deep neural network development

After obtaining the informative model parameters, a DNN is built to map the parameters to the RUL. The input of the DNN includes the parameters obtained in Eq. (6) and the output is the RUL. The DNN consists of multiple layers and neurons, and the size of the DNN can be adjusted based on the complexity of the specific task. Thus, it is flexible in model building. In this work, since we have obtained key parameters that can reflect battery degradation mechanisms, there is no need to construct a complex neural network. A fully connected neural network (FCNN) is thus implemented to model the relationship between the peak parameters and the RUL. The structure of the constructed neural network con-

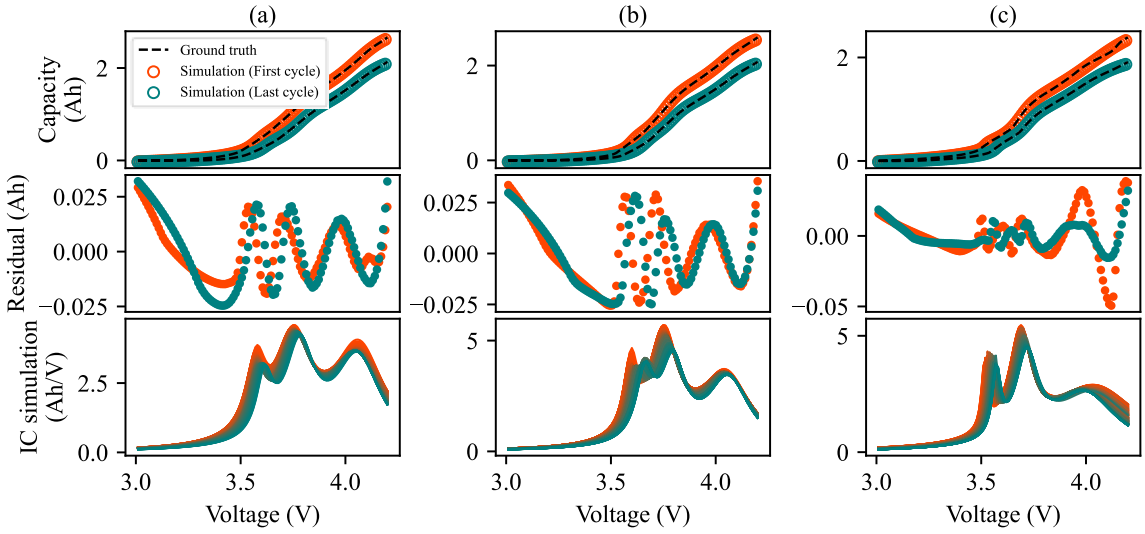

Fig. 3. The simulated Q-V curves (the first row), simulation errors (the second row), and the simulated IC curves (the last row) of the (a) NCA_25_0.5, (b) NCM_25_0.5, and (c) NCA&NCM_25_0.5 batteries. In the first two rows, the first and last cycles are taken as examples. The colour ranges from red to green as the batteries degrade.

sists of an input layer, an output layer, and two hidden layers, which can be mathematically described as follows

$$\begin{cases} h^0 = x \\ f\left(h^{j-1}\right) = w^j h^{j-1} + b^j \\ h^j = ReLU\left(f\left(h^{j-1}\right)\right) \\ z = h^l \end{cases} \quad j = 1, 2, \cdots, l \tag{8}$$

where x represents the input matrix, $f(\cdot)$ refers to the mapping between the adjacent layers, h^j is the output at the layer j where $h^0 = x$, and w^j and b^j are the weight matrix and the constant bias at the layer j. $ReLU(a) = max(0, a)$ is the active function to enhance nonlinearity, l is the number of layers (excluding input layer), and z is the final output which equals to h^l. The output of the former layer serves as the input of the latter layer in a stacked-layer structure. The neurons of the two hidden layers are set to be 256 and 128, respectively. The developed DNN maps the degradation-correlated parameters of each cycle only to the corresponding RUL in our instance. The specific model parameters are summarised in Table S3 for reference.

The built model is trained to obtain the optimal parameters by minimising the loss between the real and output values, which is calculated as follows

$$\mathscr{L} = \frac{1}{m}\sum_{i=1}^{m}\left(z_i - \hat{z}_i\right)^2 \tag{9}$$

where z_i and $\hat{z}_i$ refer to the real and output values for sample i, and m is the number of cycles. As shown in Fig. 2, the inputs are split into training and validation streams to update model parameters and hyperparameters using the feedback from training loss and validation loss, respectively. The update of the model parameters is realised by the Adam optimiser [49]. The parameters are optimised after a mini-batch of data is fed into the network, and the batch size is set to be 64. It is recognised as completing the model training if the validation loss does not decrease in ten epochs. The model is constructed using the Keras framework on a laptop configured with an AMD Ryzen 76800H CPU and an NVIDIA RTX 3060 GPU.

4. Method validation and discussion

We comprehensively validate the proposed method by considering critical factors such as temperature, current rate, and battery chemistry. The data from seven different charging situations calculated by Eq. (5) are used for training and testing datasets. We use the data collected from a battery experiencing each charging situation for testing while the data collected from other batteries are used to develop the model. The detailed training data and testing data are summarised in Table S4. In particular, 20% of the training dataset is used for validation during the model training to avoid overfitting. All the input data are pre-processed by the minimum–maximum normalisation method to scale the data into [0, 1]. The RMSE and MARE are used to evaluate the overall performance of the proposed method. The MARE is calculated as follows

$$\text{MARE} = \frac{1}{m}\sum_{i=1}^{m}\frac{\left|z_i - \hat{z}_i\right|}{z_{\text{bof}}} \tag{10}$$

where z_{bof} is the RUL at the beginning of battery life, which refers to the cycle life of a fresh battery.

We compare the proposed method with two state-of-the-art RUL prediction methods. The first one is the end-to-end method, whose input is the raw charging data. The raw data here refers to the capacity sampled at a given voltage step without further processing, which is denoted by Q in Eq. (5). It capitalises on the automatic feature extraction mechanism of deep learning but disregards the information on battery physics. The other method takes the features proposed by Severson et al. [25] as input, who demonstrated that the difference between the Q-V curves at the 100th and 10th cycles can enable accurate life prediction even before the evident capacity loss. Since the RUL is predicted at every cycle in our case, we use the difference between the Q-V curves at the cycle i ($i > 10$) and the 10th cycle here, denoted as ΔQ_{i-10}. The capacity is calculated in the same as Q in Eq. (5). ΔQ_{i-10} is a statistical feature that does not interpret ageing mechanisms in physical perspectives. The split of training and testing datasets for the proposed method remains consistent with the raw data and ΔQ_{i-10}-based methods.

4.1. RUL prediction under different charging conditions

We first validate the proposed method with three types of batteries operated under temperatures of 25, 35, and 45 °C with different current rates of 0.25 and 0.5 C. The RUL prediction results and error statistics are shown in Fig. 4. It shows that the proposed method outperforms the raw data-based and ΔQ_{i-10}-based methods in terms of RUL prediction robustness and accuracy. The errors of the former two methods are especially large in the conditions of NCA_25_0.25, NCA_45_0.5, and NCM_25_0.5, although they can track well with the actual RUL in other cases. In comparison, the proposed method exhibits robust RUL prediction under all conditions. The results also suggest that battery degradation trajectories are influenced by current rate, temperature, and battery materials, making RUL prediction challenging. The RUL prediction under NCA_25_0.25 condition fluctuates more greatly than that under other operating conditions, indicating that the current rate affects the prediction results more compared with temperature. The RMSE and MARE of the three methods are summarised in Table 2. It demonstrates that the overall accuracy of the proposed method is superior to the other methods in most cases. The average RMSE of the raw data-based and ΔQ_{i-10} based methods is 21.45 cycles and 20.92 cycles, respectively. The average MARE of both the raw data-based and ΔQ_{i-10} based methods is 5.71%. In contrast, the average RMSE and MARE of the proposed method are 11.42 cycles and 3.19%, which are reduced by 47% and 44% compared to the raw data-based method and by 45% and 44% compared to the ΔQ_{i-10}-based method, respectively.

4.2. RUL prediction using partial charging curves

Our results show that accurate RUL predictions can be made using data from only one cycle. While this is much more efficient than most existing RUL prediction models [21], one should note that the batteries do not always experience full charging in practical applications [50]. This situation is more challenging for RUL prediction as less information is available. Therefore, this section further explores the feasibility of the proposed methods in terms of partial charging situations. Since the peaks of the IC curve contain rich ageing information, this work divides the charging process into three ranges to cover three peaks. Based on the peak ranges identified in Section 3.2.2, the charging process is divided into three voltage pieces [3.0, 3.7], [3.6, 3.9], and [3.9, 4.2] V, which cover peak 1, peak 2, and peak 3, respectively.

Eq. (4) is used to model each of the three charging ranges and n is set to be 1 here. The NLS method is exploited to identify the model parameters, and the parameter boundaries are summarized in Table S5. The Q-V and IC curves of the three ranges, taking the NCA_25_0.5 condition as an example, are reconstructed in Fig. S4. The reconstructed errors are within 10 mAh, which indicates that the model can well characterise the charging process

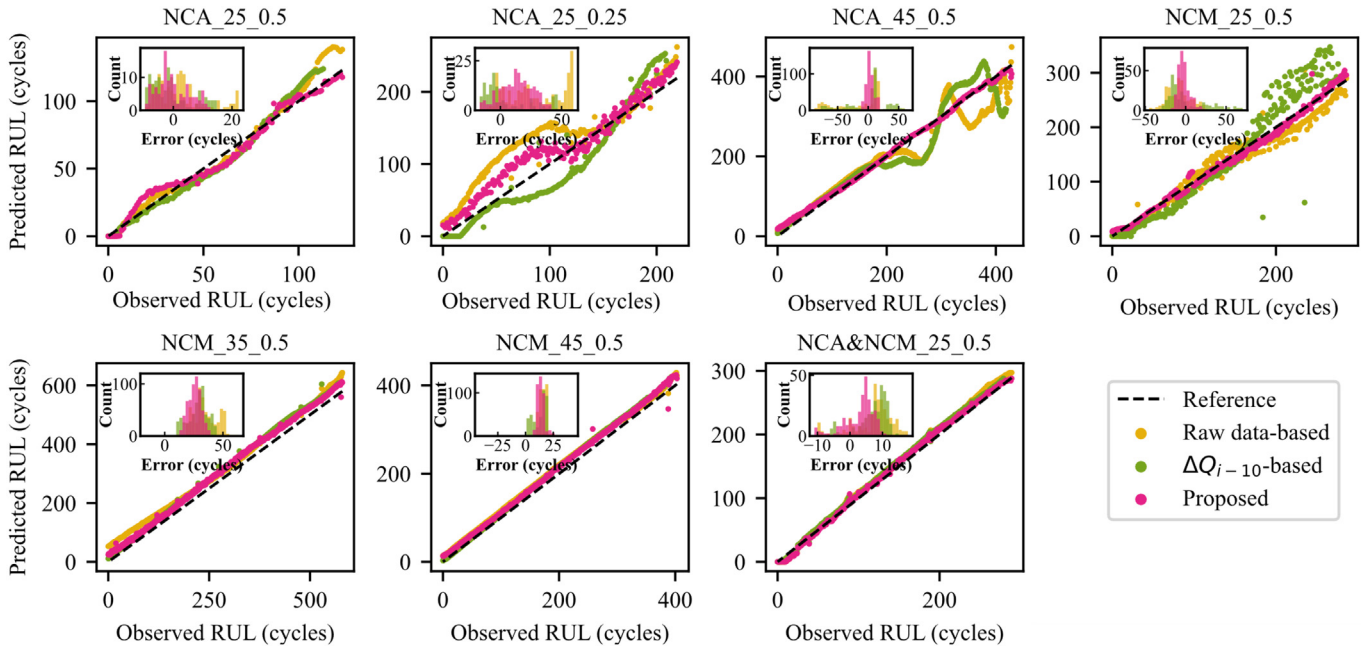

Fig. 4. The RUL predictions of the three methods under seven conditions. The insets show the histogram of the absolute errors of the three methods.

Table 2
The RMSE and MARE of RUL predictions.

Conditions	RMSE (cycles)			MARE (%)		
	Raw data	ΔQ_{i-10}	Proposed	Raw data	ΔQ_{i-10}	Proposed
NCA_25_0.5	8.24	6.84	**5.43**	4.86	5.06	**3.67**
NCA_25_0.25	35.65	25.22	**18.60**	13.09	10.22	**7.16**
NCA_45_0.5	38.88	38.06	**7.14**	6.92	6.86	**1.21**
NCM_25_0.5	17.39	35.86	**8.09**	4.99	9.47	**2.20**
NCM_35_0.5	36.48	29.97	**26.36**	6.05	5.03	**4.44**
NCM_45_0.5	16.24	**14.22**	14.44	3.95	**3.28**	3.46
NCA&NCM_25_0.5	9.37	8.61	**5.64**	2.92	2.88	**1.70**
Average	21.45	20.92	**11.42**	5.71	5.71	**3.19**

Note: the bold number indicates the lowest value for the given case.

over the battery life. We further quantify the RMSE and R^2 values of every cycle under all conditions, which are summarised in Fig. S5.

The identified model parameters, which contain the peak information, are fed into the DNN developed in Section 3.3. The raw data and Q_{i-10} features are used for comparison. The overall RUL prediction errors under the seven operational conditions are shown in Fig. 5. The results indicate that the proposed method outperforms the other two data-driven methods. In particular, the raw data-based and Q_{i-10}-based methods perform worse under the NCA_25_0.25, NCA_45_0.5, NCM_25_0.5, and NCM_35_0.5 conditions, while the proposed method still has a satisfied performance. We further summarise the RMSE and MARE of the two traditional methods in fully charged cases and those of the three methods in partially charged cases in Tables S6 and S7. The average RMSE of the proposed method under three partially charged conditions is 15.10 cycles, 17.11 cycles, and 15.98 cycles, respectively, while that of the raw data-based and the Q_{i-10}-based methods under fully charged conditions is 20.45 cycles and 20.92 cycles, respectively. The average MARE of the proposed method under three partially charged conditions is 3.78%, 4.61%, and 4.03%, respectively, while that of the raw data-based and the Q_{i-10}-based methods using fully charged curves is 5.71%. It demonstrates that the proposed method outperforms the two traditional methods overall under both fully charged and partially charged situations.

4.3. Comprehensive performance assessment

While most of the RUL prediction research only focuses on prediction accuracy, it should be noted that other indicators, including efficiency, input burden, and robustness, are important in reality. The average RMSE obtained in Sections 4.1 and 4.2 serves as the accuracy indicator. On this basis, the efficiency determines the output resolution and a higher efficiency can promptly provide battery lifetime information. The input burden presents the sophistication of data processing. A lower dimension of data is less time-consuming to analyse and pre-process. Robustness can describe the fluctuation of the outputs and score the generalisation of the proposed method applied in different situations.

Specifically, these metrics are defined as follows.

Efficiency: It is the computing time with specific configurations at each cycle given the same computing software and hardware. The parameter identification based on NLS is also taken into account for the proposed method. In general, this step is much more efficient compared with the DNN, requiring less than 0.02 ms.

Input burden: It is the number of features of the input data for RUL prediction at each cycle.

Robustness: It is evaluated by the variance of the RUL prediction errors over a battery life.

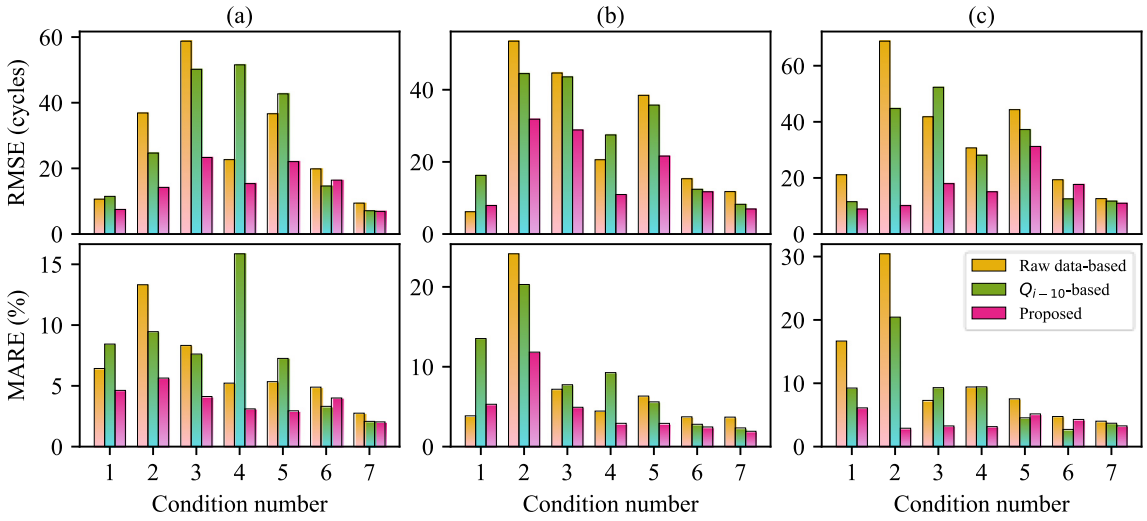

Fig. 5. The RMSE and MARE of the RUL predictions using the three peak parameters of (a) peak 1, (b) peak 2, and (c) peak 3. Condition number 1 to 7 corresponds to NCA_25_0.5, NCA_25_0.25, NCA_45_0.5, NCM_25_0.5, NCM_35_0.5, NCM_45_0.5, NCA&NCM_25_0.5 conditions, respectively.

Table 3
Comprehensive comparison of three methods in terms of four indicators.

Indicators	Methods	Full curves	Partial charging curves		
			Peak 1	Peak 2	Peak 3
Calculating time (ms)	Raw data-based	3.43	3.48	3.74	3.43
	ΔQ_{i-10}-based	3.46	3.33	3.80	3.46
	Proposed	**2.85**	**2.79**	**2.85**	**2.85**
Number of input data point	Raw data-based	121	70	30	30
	ΔQ_{i-10}-based	121	70	30	30
	Proposed	**10**	**4**	**4**	**4**
Average RMSE (cycles)	Raw data-based	21.45	27.82	27.18	34.10
	ΔQ_{i-10}-based	20.92	28.89	26.87	28.30
	Proposed	**11.42**	**15.10**	**17.11**	**15.98**
Variance of the errors (cycles)	Raw data-based	329.87	688.96	314.76	528.76
	ΔQ_{i-10}-based	486.53	552.62	314.76	327.21
	Proposed	**54.45**	**177.50**	**232.91**	**108.52**

Note: the bold number indicates the lowest value for the given case.

The values of the four indicators are summarised in Table 3, indicating that the proposed method has a shorter calculating time, fewer input parameters, higher accuracy, and higher robustness than the other two methods under the same condition.

We further evaluate the performance of the three methods by scaling the four indicators to [0, 1]. Less calculating time, average errors, and error variance indicate higher scores of efficiency, accuracy, and robustness, respectively, while fewer input parameters refer to a lower input burden score. The overall performance of the three methods is intuitively compared in Fig. 6. It demonstrates that the proposed method outperforms the raw data-based and the Q_{i-10}-based methods in both fully charging and partially charging situations. The proposed method is more accurate and robust in fully charged conditions than in partially charged conditions since the former contains more peak information. The proposed method has fewer input parameters than the other two methods, which is only 1/12 of the later ones in a fully charged case. Therefore, the proposed method has a lower input burden and a higher calculating efficiency.

4.4. Rationalisation of predictive performance

We explain the success of the proposed method from an electrochemical perspective. As the IC curves can reflect the battery degradation evolution, which constitutes LAM for two electrodes and LLI during the phase transition, we plotted the IC curves and identified the parameters of the three types of batteries in Fig. 7. It demonstrates that both IC curves and identified parameters have a strong relationship with battery degradation. Furthermore, they exhibit distinct patterns based on various battery types, which is in line with the fact that the degradation behaviour of the battery is governed by the materials and operating conditions. Altogether, the variation of ω, A, and V_o is aligned with that of the peak's width at half-height, area, and symmetric centre of IC curves. Hence, the identified parameters possess the potential to showcase the mechanisms of battery degradation. Specifically, ω is related to the interaction of active materials, which can reflect the LAM and LLI; A represents the total charged capacity that can indicate the LAM and LLI; and V_o is determined by the reversibility of the electrode reaction, which can describe the LAM. In addition, the shift of the peak potential calculated by $h = 2A/\pi\omega$ can reflect the growth of the solid electrolyte interface (SEI). Fig. 7 shows that the parameters of each peak vary in their own patterns, which results in complex battery dynamics. However, the overall trend of each type of parameter, as shown in Fig. S6, is consistent across the three types of batteries. The underlying understanding of the parameters facilitates the success of our physics-based DL method for RUL prediction.

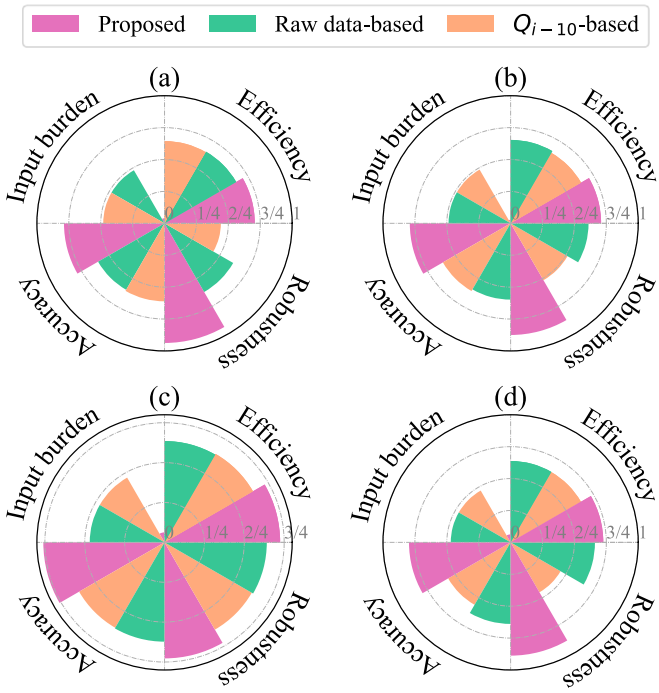

Fig. 6. The score of the three RUL prediction methods assessed in aspects of efficiency, input burden, accuracy, and robustness under four situations of (a) fully charged, (b) charging curves cover peak 1, (c) charging curves cover peak 2, and (d) charging curves cover peak 3. The input burden of the proposed method is too small to illustrate.

Though the IC curves are extensively used to investigate degradation mechanisms, their three drawbacks cannot be neglected. First, their computation requires low-rate diagnostic tests since a high charging rate will result in heterogeneous de/intercalation, thereby smearing out features [51]. It is challenging to achieve it in practical applications. Second, it will cause the signal-to-noise ratio reduction during the differential process [52]. Despite additional filtering methods to suppress the amplified noise caused by differentiation, the initial data are corrupted to some certain extent. Third, it is difficult to decouple the features of each peak from an IC curve since the peaks overlap. Thus, it is challenging to accurately acquire feature values. In contrast, the proposed method circumvents these issues and provides information on intrinsic doubled peaks, thereby constituting a more practical approach.

5. Conclusions

Deep learning-based RUL prediction can be enabled by using battery charging data as input. However, it ignores intrinsic battery ageing mechanisms. In this study, a physics-informed machine learning method is proposed to enhance the RUL prediction performance. First, a physics-based model containing physically meaningful parameters is developed to describe charging curve variation caused by degradation. The parameters represent the peak information of the IC curves, which are inherently correlated with battery degradation. Then, the parameters are identified using the NLS method based on raw operational data. A DNN is developed subsequently, which maps the ageing correlated parameters to the RUL. The method is first validated under three temperatures and two current rate situations using fully charged curves. Two traditional methods, relying on deep learning-captured features and physical-uninformed features, are compared to the proposed method. The average RMSE of the two traditional methods is 21.45 cycles and 20.95 cycles, and the average MARE is 5.71%. The RMSE and MARE of the proposed method are 11.42 cycles and 3.19% on average, which are reduced by more than 45% and 44%, respectively, compared to the other two methods. Considering the field application conditions, the partial charging curve that covers only an IC peak is further used to validate the proposed method. In this case, the proposed method outperforms the other two methods. In addition, we also evaluate the accuracy, efficiency, input burden, and robustness of the three methods. The results demonstrate that the proposed method is superior to the other two methods overall. Moreover, the inherent connections between

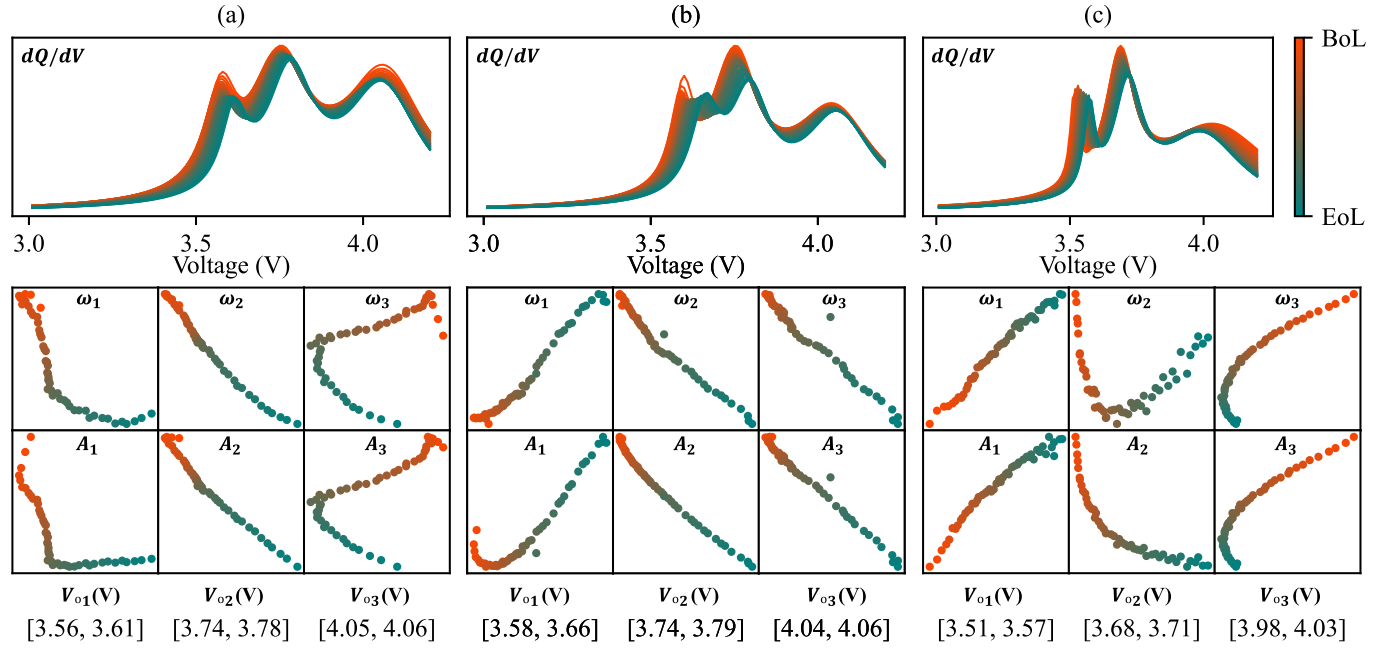

Fig. 7. The IC curves and parameters of (a) NCA, (b) NCM, and (c) NCA&NCM batteries over battery life. The *x*-axes of the parameter figure is V_o while the *y*-axes are ω and *A*, respectively. The colour is scaled according to the RUL. Since the parameters need to be normalised before being fed into the FCNN, their values are not displayed here.

the identified parameters and battery degradation evolution are analysed, explaining how the domain knowledge helps with deep learning for RUL prediction.

There are two contributions in this study. First, the proposed method integrates domain knowledge into deep learning, enhancing the RUL prediction of the traditional data-driven methods with raw data or statistical features. We validate this by comparing the proposed method with two state-of-the-art methods. Second, the method is generalisable to various operating conditions such as different charging rates, temperatures, materials, and both full and partial charging processes. Overall, our work reveals that it is important to take battery physics into account when implementing data-driven models for predicting battery degradation. Further investigation into different data and knowledge integration approaches will be an interesting research direction based on this work.

Declaration of competing interest

The authors declare that they have no known competing financial interests or personal relationships that could have appeared to influence the work reported in this paper.

Acknowledgments

J. Tian acknowledges the financial support from the National Natural Science Foundation of China (52207229). L. Ma acknowledges the financial support from the China Scholarship Council (202207550010).

Appendix A. Supplementary data

Supplementary data to this article can be found online at https://doi.org/10.1016/j.jechem.2023.12.043.

References

[1] Y. Ding, Z.P. Cano, A. Yu, J. Lu, Z. Chen, Electrochem. Energy Rev. 2 (2019) 1–28.
[2] S. Liu, Y. Nie, A. Tang, J. Li, Q. Yu, C. Wang, eTransportation 18 (2023) 100296.
[3] M. Dubarry, D. Beck, Accounts Mater. Res. 3 (2022) 843–853.
[4] S. Ji, J. Zhu, Z. Lyu, H. You, Y. Zhou, L. Gu, J. Qu, Z. Xia, Z. Zhang, H. Dai, J. Energy Chem. 78 (2023) 565–573.
[5] J. Zhu, W. Xu, M. Knapp, M.S. Dewi Darma, L. Mereacre, P. Su, W. Hua, X. Liu-Théato, H. Dai, X. Wei, H. Ehrenberg, Cell Reports Phys. Sci. 4 (2023) 101464.
[6] X. Liu, H. Peng, B. Li, X. Chen, Z. Li, J. Huang, Q. Zhang, Angew. Chemie Int. Ed. 61 (2022) e202214037.
[7] S.J. Harris, D.J. Harris, C. Li, J. Power Sources 342 (2017) 589–597.
[8] S. Zhou, X. Zhang, C. Chen, M. Chen, F. Kong, Y. Qiao, J. Wang, J. Energy Chem. 83 (2023) 98–105.
[9] H. You, J. Zhu, X. Wang, B. Jiang, H. Sun, X. Liu, X. Wei, G. Han, S. Ding, H. Yu, W. Li, D.U. Sauer, H. Dai, J. Energy Chem. 72 (2022) 333–341.
[10] S. Ansari, A. Ayob, M.S. Hossain Lipu, A. Hussain, M.H.M. Saad, Energy Reports 8 (2022) 12153–12185.
[11] S. Han, Y. Tang, S. Khaleghi Rahimian, J. Power Sources 490 (2021) 229571.
[12] H. Hinz, Inventions 4 (2019) 41.
[13] X. Han, M. Ouyang, L. Lu, J. Li, J. Power Sources 268 (2014) 658–669.
[14] C. Lyu, Q. Lai, T. Ge, H. Yu, L. Wang, N. Ma, Energy 120 (2017) 975–984.
[15] A. Guha, A. Patra, IEEE Trans. Instrum. Meas. 67 (2018) 1836–1849.
[16] L. Shao, Y. Zhang, X. Zheng, X. He, Y. Zheng, Z. Liu, Energies 16 (2023) 1469.
[17] X. Liu, X.-Q. Zhang, X. Chen, G.-L. Zhu, C. Yan, J.-Q. Huang, H.-J. Peng, J. Energy Chem. 68 (2022) 548–555.
[18] S. Ji, M. Dai, H. Wen, H. Zhang, Z. Zhang, Z. Xia, J. Zhu, Int. J. Adv. Manuf. Technol. 122 (2022) 3149–3159.
[19] S. Ji, J. Zhu, Y. Yang, H. Zhang, Z. Zhang, Z. Xia, Z. Zhang, Micromachines 13 (2022) 847.
[20] J. Zhu, S. Ji, Z. Ren, W. Wu, Z. Zhang, Z. Ni, L. Liu, Z. Zhang, A. Song, C. Lee, Nat. Commun. 14 (2023) 2524.
[21] X. Li, D. Yu, V. Søren Byg, S. Daniel Ioan, J. Energy Chem. 82 (2023) 103–121.
[22] T. Han, J. Tian, C.Y. Chung, Y. Wei, J. Energy Chem. 89 (2024) 434–436.
[23] H. Meng, M. Geng, T. Han, Reliab. Eng. Syst. Saf. 236 (2023) 109288.
[24] V. Sawant, R. Deshmukh, C. Awati, J. Energy Chem. 77 (2023) 438–451.
[25] K.A. Severson, P.M. Attia, N. Jin, N. Perkins, B. Jiang, Z. Yang, M.H. Chen, M. Aykol, P.K. Herring, D. Fraggedakis, M.Z. Bazant, S.J. Harris, W.C. Chueh, R.D. Braatz, Nat. Energy 4 (2019) 383–391.
[26] Z. Zhou, D.A. Howey, IFAC-PapersOnLine 56 (2023) 6117–6123.
[27] J. Wang, C. Zhang, L. Zhang, X. Su, W. Zhang, X. Li, J. Du, Energy 273 (2023) 127169.
[28] D. Roman, S. Saxena, V. Robu, M. Pecht, D. Flynn, Nat. Mach. Intell. 3 (2021) 447–456.
[29] H. Jiang, H. Wang, Y. Su, Q. Kang, X. Meng, L. Yan, T. Ma, J. Power Sources 542 (2022) 231818.
[30] C. Wang, R. Xiong, J. Tian, J. Lu, C. Zhang, Appl. Energy 305 (2022) 117819.
[31] C.-W. Hsu, R. Xiong, N.-Y. Chen, J. Li, N.-T. Tsou, Appl. Energy 306 (2022) 118134.
[32] J. Tian, R. Xiong, W. Shen, J. Lu, EcoMat 4 (2022) 1–12.
[33] J. Tian, R. Xiong, J. Lu, C. Chen, W. Shen, Energy Storage Mater. 50 (2022) 718–729.
[34] A. Daw, A. Karpatne, W.D. Watkins, J.S. Read, V. Kumar, in: Knowledge-Guided Mach. Learn., Chapman and Hall/CRC, Boca Raton, 2022, pp. 353–372.
[35] J. Zhu, Y. Wang, Y. Huang, R. Bhushan Gopaluni, Y. Cao, M. Heere, M.J. Mühlbauer, L. Mereacre, H. Dai, X. Liu, A. Senyshyn, X. Wei, M. Knapp, H. Ehrenberg, Nat. Commun. 13 (2022) 2261.
[36] Z. Deng, X. Hu, Y. Xie, L. Xu, P. Li, X. Lin, X. Bian, iScience 25 (2022) 104260.
[37] C. Lin, J. Xu, M. Shi, X. Mei, Energy 247 (2022) 123556.
[38] J. Chen, Y. Hu, Q. Zhu, H. Rashid, H. Li, Energy 282 (2023) 128782.
[39] S.M. Hell, C.D. Kim, Batteries 8 (2022) 192.
[40] C. Hu, L. Ma, S. Guo, G. Guo, Z. Han, Energy 246 (2022) 123404.
[41] Y. Yang, L. Zhao, Q. Yu, S. Liu, G. Zhou, W. Shen, J. Energy Storage 70 (2023) 108037.
[42] T. Han, Z. Wang, H. Meng, J. Power Sources 520 (2022) 230823.
[43] J. Tian, R. Xiong, W. Shen, J. Lu, F. Sun, Energy Storage Mater. 51 (2022) 372–381.
[44] J. Lu, R. Xiong, J. Tian, C. Wang, C. Hsu, N. Tsou, F. Sun, J. Li, Energy Storage Mater. 50 (2022) 139–151.
[45] P. Liu, Y. Wu, C. She, Z. Wang, Z. Zhang, IEEE Trans. Power Electron. 37 (2022) 12563–12576.
[46] J. Guo, Y. Li, J. Meng, K. Pedersen, L. Gurevich, D.-I. Stroe, J. Energy Chem. 74 (2022) 34–44.
[47] G. Seo, J. Ha, M. Kim, J. Park, J. Lee, E. Park, S. Bong, K. Lee, S.J. Kwon, S. Moon, J. Choi, J. Lee, J. Energy Chem. 67 (2022) 663–671.
[48] J. He, X. Bian, L. Liu, Z. Wei, F. Yan, J. Energy Storage 29 (2020) 101400.
[49] L. Ma, C. Hu, F. Cheng, J. Energy Storage 37 (2021) 102440.
[50] J. Tian, R. Xiong, W. Shen, J. Lu, X.-G. Yang, Joule 5 (2021) 1521–1534.
[51] M. Lewerenz, A. Marongiu, A. Warnecke, D.U. Sauer, J. Power Sources 368 (2017) 57–67.
[52] R.R. Richardson, C.R. Birkl, M.A. Osborne, D.A. Howey, IEEE Trans. Ind. Informatics 15 (2019) 127–138.